

# Contents

<b>1 TJ-Monopix 2</b>	<b>4</b>
1.1 Matrix and flavors . . . . .	4
1.1.1 Flavors . . . . .	5
1.1.2 Pixel design . . . . .	6
1.1.2.1 Improved front-end circuit design . . . . .	7
1.2 Threshold and noise . . . . .	8
1.2.1 S-Curve method . . . . .	8
1.2.1.1 Normal FE . . . . .	9
1.2.1.2 Cascode FE . . . . .	9
1.2.1.3 HV-Cascode FE . . . . .	10
1.2.1.4 HV-Normal FE . . . . .	12
1.2.1.5 Summary Table . . . . .	13
1.2.2 Threshold dispersion and tuning . . . . .	15
1.2.2.1 Results from fine tuning . . . . .	16
1.3 ToT calibration with internal injection . . . . .	16
1.3.1 Injection circuit issues . . . . .	16
1.3.2 Time Over Threshold (TOT) curves and fit . . . . .	17
1.4 Response to radioactive source and absolute calibration . . . . .	18
1.4.1 $^{55}\text{Fe}$ . . . . .	19
1.4.2 $^{241}\text{Am}$ . . . . .	19
1.4.3 $^{109}\text{Cd}$ . . . . .	21
1.4.4 Injection capacitance calibration . . . . .	21

1.4.5	Check on linearity of tot fit . . . . .	24
1.5	Operation with low threshold . . . . .	24
1.5.1	Register optimization . . . . .	26
1.5.2	Comparison between data and simulation . . . . .	27
1.5.2.1	$I_{CASN}$ . . . . .	27
1.5.2.2	$I_{THR}$ . . . . .	28
1.5.2.3	Time over Threshold (ToT) . . . . .	30
1.5.2.4	some nice picture of the optimized thr and tuning	30
1.6	Cross talk issue and mitigation . . . . .	31
1.6.1	Hot pixel issue and strategy? . . . . .	31
1.6.2	Readout sequence . . . . .	31
1.6.3	Hot pixel strategy (study) . . . . .	31
1.6.4	Cross-talk . . . . .	31
1.6.5	Mitigation . . . . .	31
1.7	Test Beam results . . . . .	31

**2 Conclusions** **32**

## **Abstract**

# 1. TJ-Monopix 2

In the previous chapter we have seen the fundamental steps that had lead to the development of the CMOS MAPS sensors thechnology and the history of their many different prototypes.

Here we will go through the main features of TJ-Monopix 2, which represents the improvement of its predecessor TJ-Monopix 1, conceived(designed) to address efficiency degradation after irradiation. The characterization of the chip has crucial consequences in the VTX upgrade program and therefore in the evolution of the OBELIX (sensor).

The chip W14R12 (1.1 on the facing page) wihch is one of the matrices tested during the Test Beam in Desy (July 2022) has been fully characterize in Pisa and in particular several aspects have been analyzed, among which:

- TOT calibration by internal charge injection;
- characterization with radioactive sources;
- systematic study of different registers settings in order to operate the chip with lower thresholds;
- investigation of an important issue with cross talk, due to digital signal from the readout, discovered operating at lower threshold (below  $250 e^-$ ).

This well-structured study returned relevant results which have helped in TestBeam data reconstruction and in the simulations SW(???) of the upgraded VTX with CMOS MAPS devices.

## 1.1 Matrix and flavors

Tj-Monopix 2 is the next generation small collection electrode DMAPS prototype in TowerJazz 180 nm. The need to create a sensor capable to mantain high efficiency even after irradiation, required improvements compared to Tj-Monopix 1 in two important fields: a lower operating threshold and different pixel layout to increase charge collection efficiency all over its area, expecially in the corners.

To achieve these goals, a different front-end in pixel circuit was implemented and a lot of efforts have been focused on optimizing pixel layout in order to reduce its size which has been decreased to  $33.04 \times 33.04 \mu m^2$ . As a matter of fact we have seen in (REFERENCE) that pixel's diensions are critical to accomplish faster charge collection across all active area, increasing the lateral

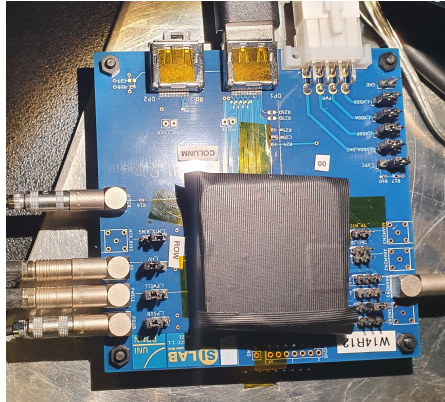


Figure 1.1: The W14R12 chip tested during the Test Beam in Desy.

electric field. For this reason it was necessary a special effort to design and create a smaller pixel but still adequate to embody the full digital readout . All of this required to work at the technology density limit and also further modification at the circuit design, such as single ended data transmission in order to reduce the column-bus width.

### 1.1.1 Flavors

The prototype is a  $2 \times 2 \text{ cm}^2$  pixel matrix which consists of 512x512 pixels and all of them are designed with a reduced deep p-well geometry (RDPW) because as it was demonstrated during the testing of TJ-Monopix1, this type of structure has a superior charge collection properties compared to full deep p-well coverage (FDPW) (figure 1.2). The total active area of the matrix is approximately 286  $\text{mm}^2$ .

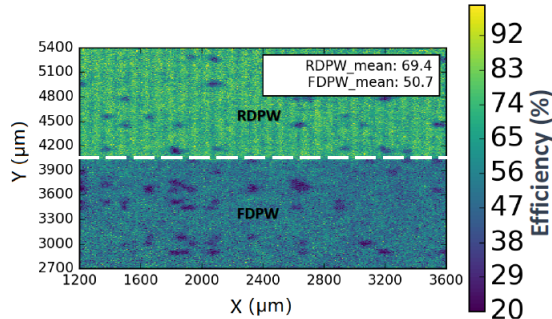


Figure 1.2: Detection efficiency map of a TJ-Monopix1 chip with 25  $\mu\text{m}$  p-epitaxial layer that has been irradiated to  $10^{15} \text{ n}_{eq}/\text{cm}^2$  NIEL.

As we can see in figure 1.3 on the following page, the matrix is divided in four sectors, named **flavors** that implement different variation of the front-end circuit. In the first two flavors the collection electrode is DC-coupled directly with the readout electronics, the continuous baseline reset is implemented by a for-

ward bias diode and they differ for the pre-amplifier circuit design. The second flavor, named **Cascode FE**, includes an extra cascode transistor that increase the pre-amplifier gain and results in 50% reduction of the threshold dispersion compared to the first flavor, the **Normal FE**. The other two flavors consist of AC-coupled pixels (through a metal-oxide-metal MOM capacitor) [with front-side HV biasing] and in particular the **HV-Cascode FE** also incorporate the aforementioned pre-amplifier variation. AC-coupling allows to apply an high positive bias voltage (HV) to the collection electrode, but at the same time it also causes signal losses mainly due to the additional parasitic capacitance introduced at the sensitive input node.

The BCID bus width has been increased to 7-bits due to higher gain and ToT slope with respect to Tj-Monopix 1.

It's worth mentioning here that the large column height (approx. 17 mm) due to large matrix area and the aggressive column-bus routing (which refers to the minimum line width and spacing) because of the smaller pixel size (always with respect to TJ-Monopix 1) generated a significant signal transmission delay due to the RC low pass filtering effect of the long metal wires. Consequently a special circuit has been planned(designed) that adds a variable delay to the hit pulse across the column that matches that of the BCID signal.

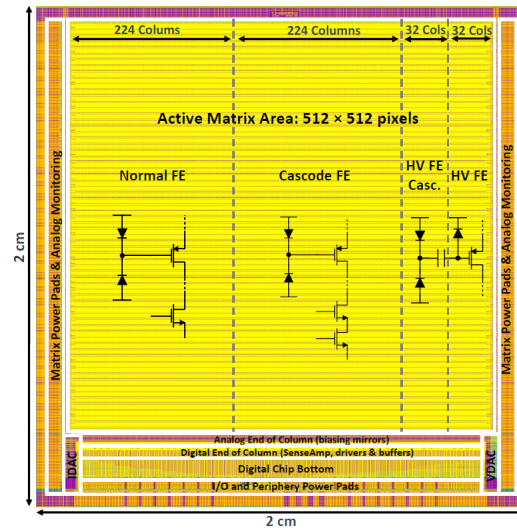


Figure 1.3: The layout of the TJ-Monopix2 prototype divided in four different flavors: **Normal**, **Cascode**, **HV-Cascode** and **HV FE**.

### 1.1.2 Pixel design

VEDI

The  $2 \times 2$  pixel core layout, shown in figure ?? on page ?? is fully optimized and is designed in order to share as much functionality as possible between the four pixels. The analog area incorporate the front-end circuit, the 3-bit threshold tuning DAC and the pixel configuration registers. The digital region

is composed by the 7-bit LE and TE memory (14 SRAM cells per pixel), the 10 bit address ROM (2 bit for the pixel position inside the core and 8 for the group address), the readout control logic and the hit delay circuit that is used to correct for the BCID propagation delay. Two different token signal are used to set the priority of the pixels during the readout: the fast one that propagates across the double column established the priority between the cores and the local one, which arbitrates the reading order of the four pixels inside each core.

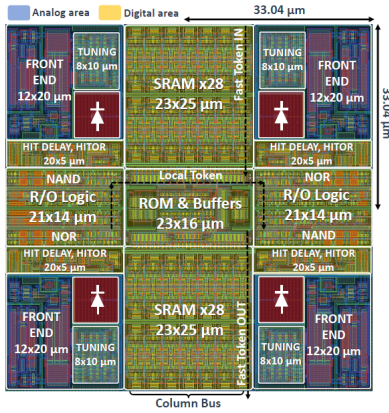


Figure 1.4: Layout of a TJ-Monopix 2 2x2 pixel core. In blue the analog area and in yellow the digital one.

### 1.1.2.1 Improved front-end circuit design

As we have seen above, there are two variations of the front-end circuit, "normal" and "cascode" type. The latter in particular includes an extra cascode transistor which increases the pre-amplifier gain and consequently reduces the threshold dispersion.

Moreover in TJ-Monopix 2 it was preferred to incorporate a simple diode to reset the input node instead of a PMOS transistor, which was the technology implemented in TJ-Monopix 1. A side effect of this choice is that the relationship between charge injected and the ToT of the detected signal is not linear anymore, because the diode is a not linear element and its discharge rate also depends on the collected charge. Indeed in the following analysis it was necessary to fit the ToT trend with a more complex function. But at the same time, the advantages are its simplicity ( $p^+$  diffusion within the n-well collection electrode) and also the fact that it allows to increase radiation tolerance to TID effects, which was one of the key working area in the upgrade of the sensor, in order to design a final(conclusive) prototype to employ in the experiments subjected to high radiation doses.[pag 153??]

In the last two AC-coupled flavors are implemented the same improvements, but here the different coupling provokes an important loss in the collected charge, as verified during the testing phase of TJ-Monopix 1 (50% losses), due at most to additional parasitic capacitances. Thus (Therefore) a lot of (many) efforts have been made to improve this aspect, working on the coupling capaci-

tor values. It reaches a signal loss of 41.5%, which is an enhancement (progress) with respect to the predecessor.

## 1.2 Threshold and noise

In order to achieve the absolute calibration of the whole matrix, the response of each pixel has been characterized by means of the internal charge injection.   
?????

The hit injection circuit included in TJ-Monopix 2 is similar to the one of TJ-Monopix 1, shown in figure(????). It allows to inject artificial hits through an injection capacitance  $C_{inj}$  connected at the collection electrode, which is equal to 230 aF for both the DC and AC coupling FE. The injected charge is almost linear with the injection pulse amplitude (set by the two registers " $V_L$ " and " $V_H$ ", like  $\Delta V_{inj} = V_H - V_L$ ). Moreover the injection step is finer compared to the one of TJ1 because of the higher voltage DAC resolution, in fact LSB (*Least Significant Bit*)=7.03 mV. The injected charge  $Q_{inj}$  can be calculated from:

$$Q_{inj} = \frac{230 \text{ aF}}{q_{e^-}} \cdot \Delta V_{inj} = 1.4375 \frac{e^-}{mV} \cdot 7.03 \frac{mV}{DAC \text{ unit}} \approx 10.1 \frac{e^-}{DAC \text{ unit}} \quad (1.1)$$

Eventually this value has been used to convert the information of the injected charge from DAC unit to electrons unit useful for further analysis.

The four flavors have been separately analyzed to be able to study their main difference concerning their performance and features, but the same method, called *s-curve method*, explained below has been used.

### 1.2.1 S-Curve method

In order to obtain the threshold and noise values for all pixels, each one of them has to be injected an arbitrary number of times (100 times in this work) for each value of the injection pulse between a minimum voltage (value), chosen setting the chip register "**VL**" and a maximum voltage (value) set by the "**VH**" register, with a step of 1 DAC unit (this is also adjustable). These two levels are provided by the voltage DAC.

So for each injection pulse height, the mean of 100 injection outputs are considered and it represents one data in the plot. In this way plotting the average number of detected hits in function of the injected charge, the typical curve better known as "*S-curve*" is reconstructed. It can be fit with the *Cumulative Distribution Function (CDF)*:

$$CDF(Q) = \frac{1}{2} \cdot \left( 1 + erf\left(\frac{Q - \mu}{\sigma \sqrt{2}}\right) \right) \quad (1.2)$$

from which the value of the threshold is evaluated considering the value of the injected charge at half of the curve's maximum height, so the parameter  $\mu$  obtained from the fit and the noise instead is evaluated from the fit parameter  $\sigma$ .  $erf(x)$  is the Gauss error function.

Specifically plotting the number of hits observed on each pixel divided by the total number of injections, for each injected charge, the half height corresponds to a charge value for which the pixel detects 50 hits of 100 injected and so when

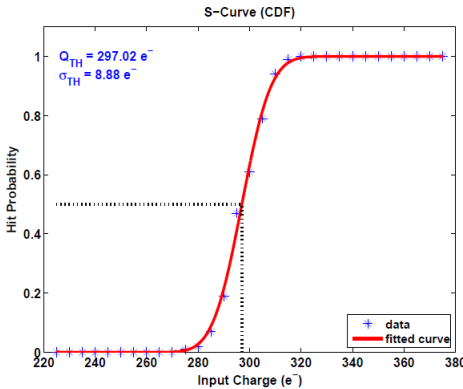


Figure 1.5: An example of the S-Curve fitted by the CDF to evaluate threshold and noise.

it has an occupancy of 0.5. In figure 1.5 is shown an example.

This method allows to study the noise and threshold of all pixels and also the threshold dispersion across an entire FE.

In the following are reported the results of this study for the flavors of all matrix, injected a charge gradually increasing from 0 to 140 DAC ( $\approx 1414 \text{ e}^-$  adopting the conversion factor in equation 1.1)

#### 1.2.1.1 Normal FE

The first flavor of the matrix is the **Normal FE**, which consist of 512 rows and 224 columns for a total of 114.688 pixels. The chip registers have been set with the same values used during the Test Beam at Desy (July 2022) which are different for the DC and AC-coupling case. They are known as "**GOE settings**" and they are reported in table 1.1 on the next page, where are also added the different biasing voltages used to power (up) the chip.

Using this setting, none of the pixels were noisy and so it wasn't necessary to use any mask. In figure 1.6 on the following page are plotted all the s-curves of the all well-functioning Normal flavor pixels. The width of the plot is a first indication (manifestation, symptom) of the threshold dispersion of the whole flavor.

The threshold and noise distributions obtained injecting all pixels as explained above, have been fitted with a gaussian distribution and they are shown in figure ?? with their maps, too.

#### 1.2.1.2 Cascode FE

**Cascode FE** is the second flavor and like **Normal FE** it consists of 512 rows and 224 columns for a number of total pixels equal to 114.688. For this flavor the same procedure of Normale FE has been followed and also the same values' registers (table 1.1 on the next page) have been used. There were not find noisy pixels. In figure ?? on page ?? the S-curves of all pixels are shown.

Registers	Normal/Cascode FE ( $P_{SUB}/P_{WELL} = -3$ V)	HV/HV-Cascode FE ( $P_{SUB}/P_{WELL} = 0$ V, HV = +5 V)
$I_{THR}$	64	30
$I_{BIAS}$	50	60
$V_{RESET}$	143	100
$I_{CASN}$	0	8
$V_{CASP}$	93	40
$V_{CASC}$	228	228
$I_{DB}$	100	100
$I_{TUNE}$	53	53
$V_{CLIP}$	255	255
$I_{COMP}$	80	80
$I_{DEL}$	88	88
$I_{RAM}$	50	50

Table 1.1: Settings of the main registers used for all flavors (W14R12 chip) during the Test Beam in Desy.

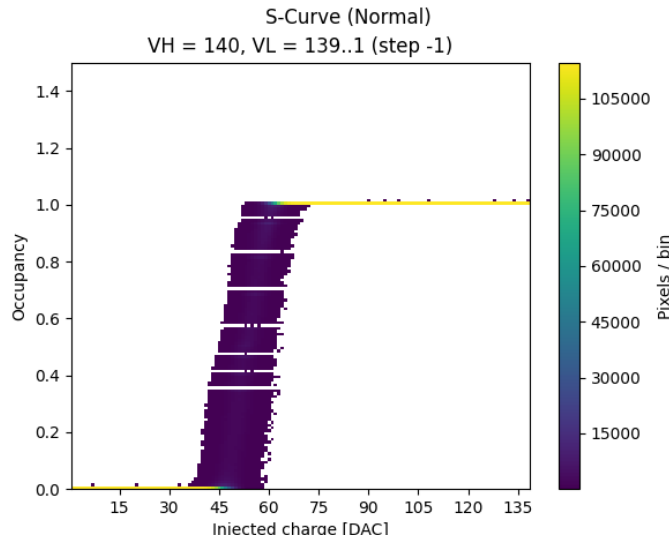


Figure 1.6: S-curves of all pixels of the Normal FE with an injection pulse of 140 DAC.

The fit of the threshold and noise distributions and maps instead, are shown in figure ?? on page ??.

### 1.2.1.3 HV-Cascode FE

The third flavor is **HV-Cascode FE** where HV stands for **High Voltage** and it is formed (counts) of 512 rows and 32 columns for a total number of pixel equal to 16384. Also for these last two flavors, the main chip registers are set with the same values tested and used during the Test Beam (@Desy) (but different from

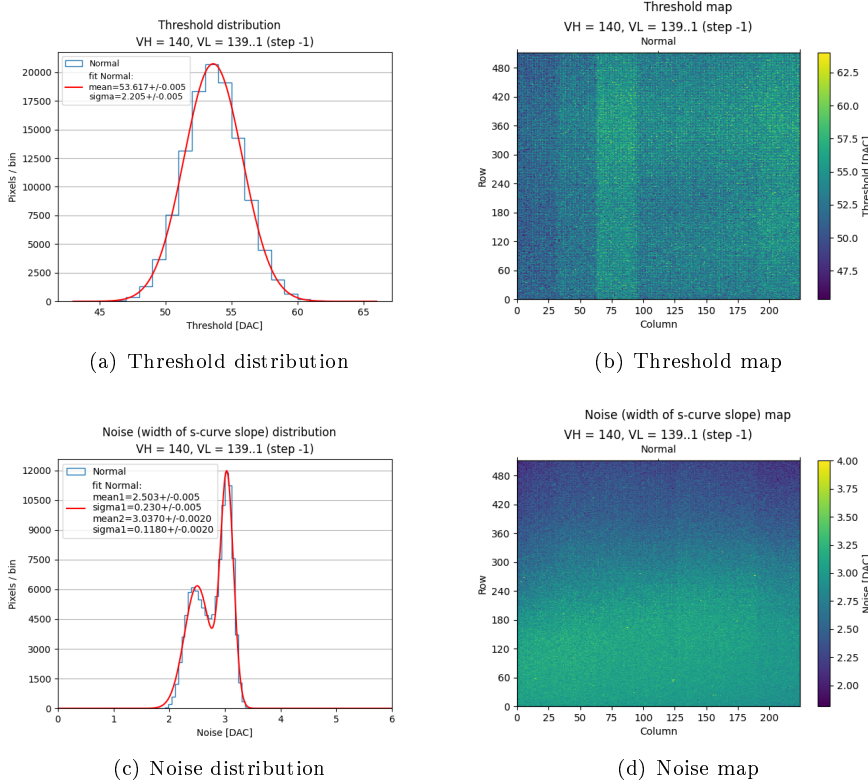


Figure 1.7: Normal FE.

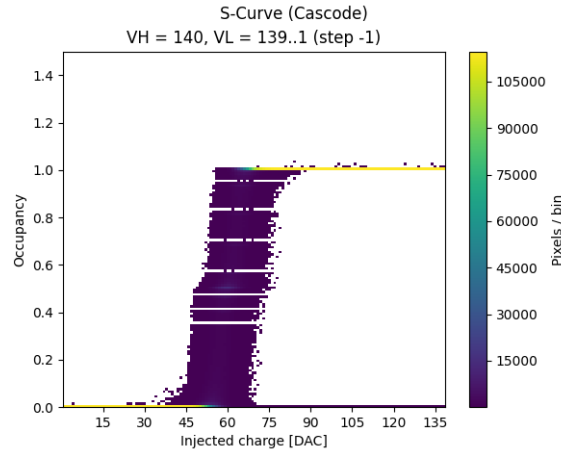


Figure 1.8: S-curves of all pixels in the **Cascade** flavor with an injection pulse of 140 DAC.

those used for the first two flavors). They are reported in table on page ?? .

As we can see from the plot of the alle S-curves in figure on page 13, there

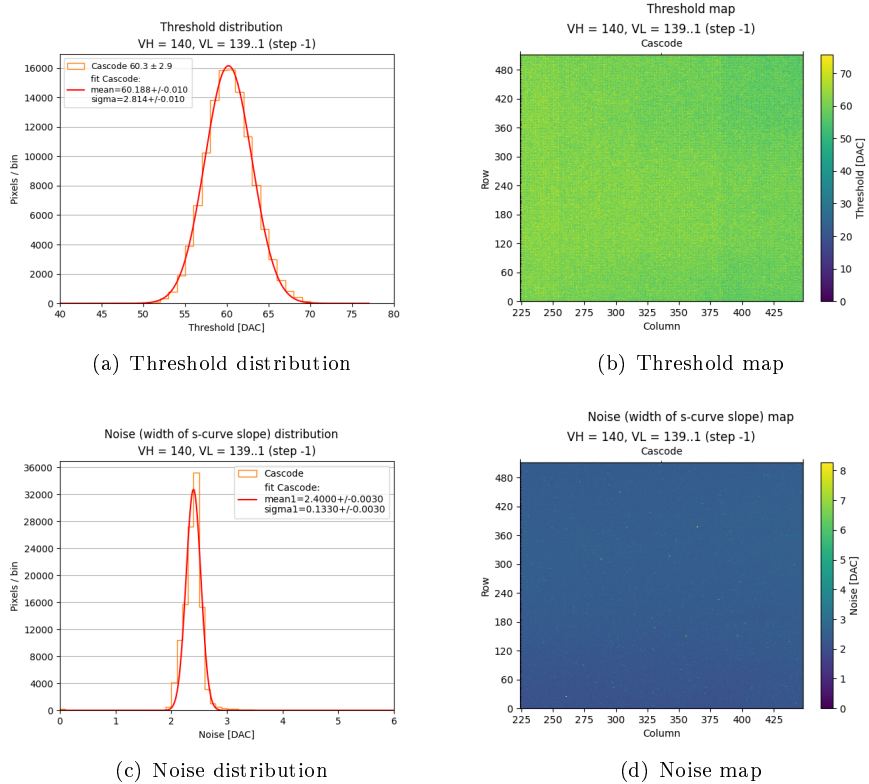


Figure 1.9: Cascode FE.

were a lot of noisy pixels with these choices of values' registers, but at this stage of measurements they were not masked. As a matter of fact along the y-axis of this plot is displayed the occupancy and when this values becomes higher than 1, it means that the pixel detects more hits than the injected ones, so it could be identified as "*noisy pixel* (because it results active regardless of the charge injection)".

In figure 1.11 on the facing page are shown the fit of the threshold and noise distributions.

#### 1.2.1.4 HV-Normal FE

The fourth and last flavor is the **HV-Normal FE** which consists of 512 rows and 32 columns for a total number of pixel equal to 16.384. The main registers have been set with the values reported in table on page ???. In figure on page 14, the S-curves of all pixel in the flavor. Also here we can see that there were some noisy pixels unmasked. Moreover, in this final flavor, the last 16 columns were not working (visible in the maps in figure on page ??) and as a matter of fact they had return a peak of threshold near the value 0, which is excluded from the threshold distributions plots.

So actually in this part of the matrix, the real number of pixel studied was the half of the total, such as 8192 pixels.

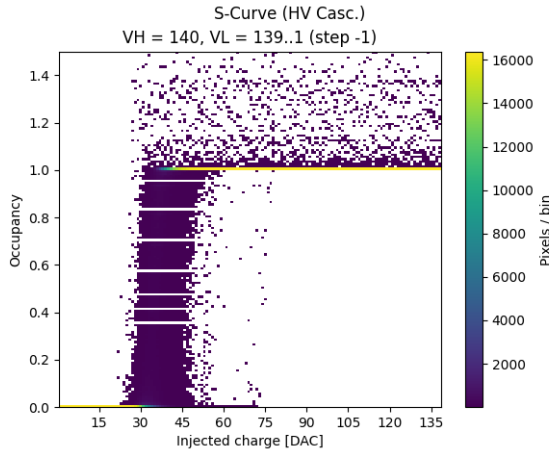


Figure 1.10: S-curves of all pixels in **HV Cascode** flavor with an injection pulse of 140 DAC.

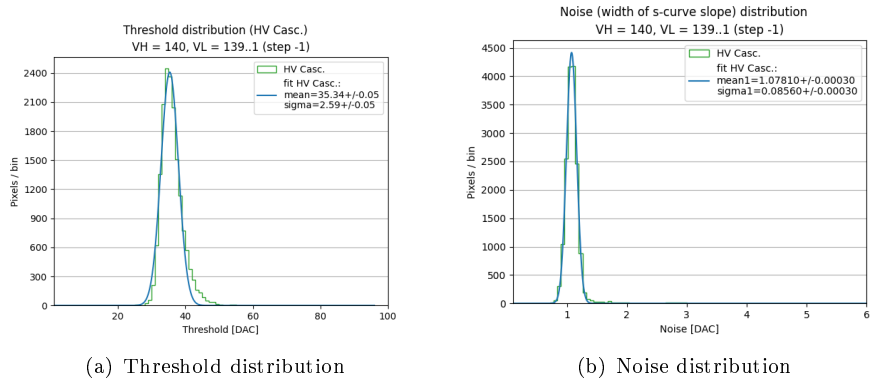


Figure 1.11: HV Cascode FE.

In figure 1.13 on the following page the fit of the threshold and noise distributions.

At last in figure on page ?? the threshold and noise maps of the whole HV flavor.

As we will see in the following (section REFERENCE), the atypical s-curves in HVs flavors have been the first hint(evidence) of the cross-talk problem (section REFERENCE) tied to a lower global threshold in these sectors with TB settings.

#### 1.2.1.5 Summary Table

In table on page ?? a summary of results for threshold, noise and threshold dispersion of all FE.

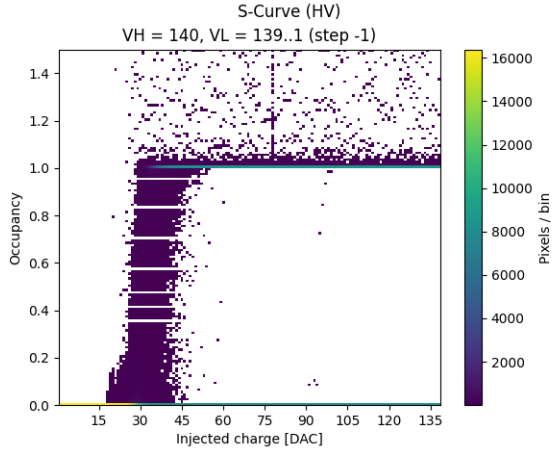


Figure 1.12: S-curves of all pixels in **HV Cascode FE** with an injection pulse of 140 DAC.

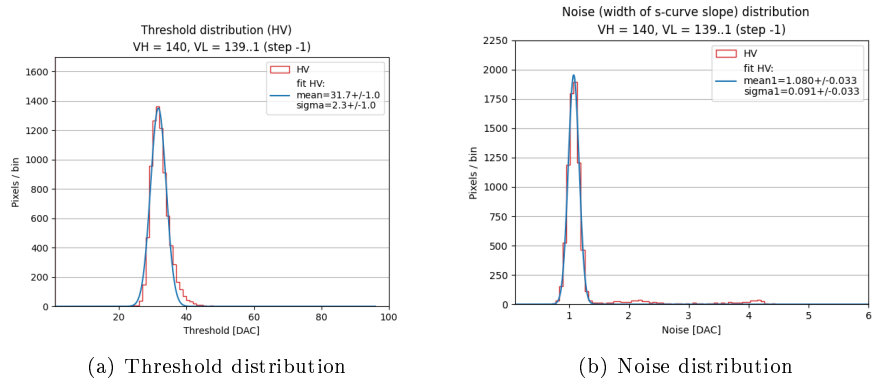


Figure 1.13: HV Normal FE.

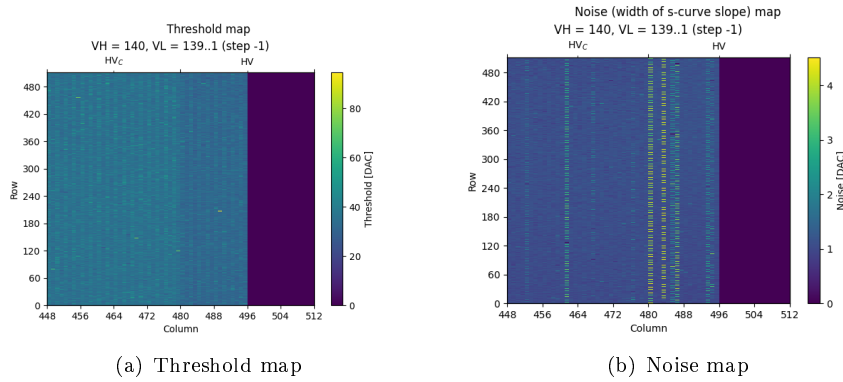


Figure 1.14: HV's FE.

Front-End	Threshold [ $e^-$ ]	Threshold dispersion [ $e^-$ ]	Noise [ $e^-$ ]
Normal	$53.62 \pm 0.01$	$2.21 \pm 0.01$	$2.503 \pm 0.005$ $3.037 \pm 0.002$
Cascode	$60.19 \pm 0.01$	$2.81 \pm 0.01$	$2.400 \pm 0.003$
HV - Cascode	$35.34 \pm 0.05$	$2.59 \pm 0.05$	$1.0781 \pm 0.0003$
HV	$31.70 \pm 0.10$	$2.30 \pm 0.10$	$1.080 \pm 0.033$

Table 1.2: Summary table of threshold and noise values for all flavors of the W14R12 chip.

### 1.2.2 Threshold dispersion and tuning

Despite its predecessor, Tj-Monopix 2 is equipped with a circuit which allows the *threshold tuning*. In other words it can adjust every pixel threshold, even if only by few DAC, in order to have a global threshold on the matrix as uniform as possible, or in any case a dispersion as small as possible, especially after irradiation. We have already noticed that (took a look to) (1.4 on page 7) the analog part of the in-pixel front-end that includes the 3-bit threshold tuning DAC, which not only improves the global threshold dispersion across the pixels, but also solves the issue with the unintentionally masked ghost pixels, reducing the noise even more. This system has been designed in order to decrease the some effects that affected the threshold dispersion like systematics (for example, related to biasing), process and temperature variations and radiation damage.

Threshold trimming of each (individual) pixel is performed with the help of a tuning DAC (TDAC), shown in figure 1.15 on the following page. In particular this component controls the discriminator active load (comparison?) current  $I_{DISC}$  which is partly(?) responsible of the pixel threshold. It works as an analog multiplexer (consisting of simple PMOS transistor switches), which selects one of seven  $I_{DISC,n}$  lines generated by the main 8-bit biasing DAC. So the possible value of the final  $I_{DISC}$  is given by the sum of two contributions:

$$I_{DISC} = I_{DISC,coarse} + (TCODE - 1) \cdot I_{DISC,fine}, \quad \text{where } 1 \leq TDAC \leq 7 \quad (1.3)$$

$I_{DISC,coarse}$  is the current set by the main(raw?) value of threshold, resulting by the setting of the main registers which are responsible for it.  $I_{DISC,fine}$  is the current selected by the fine tuning step (TDAC) and it depends on the 3-bit tuning code that is stored in the in-pixel tuning memory latch (the in-pixel configuration memory). **TCODE** is the decimal representation of the TDAC code.

For example if the 3-bit DAC are set to "111", the decimal representation is 8 and the fine tuning provide a current  $I_{DISC,7}$ , which corresponds to the highest threshold. If the 3-bit are set to "010" the corresponding TCODE is 2 and the current  $I_{DISC,1}$  is provided that set the lowest threshold possible around the central value  $I_{DISC,coarse}$ . The particular combination "000" instead (TCODE = 0) masks the pixel by disabling the discriminator, without affects the functioning(operation) of the others.

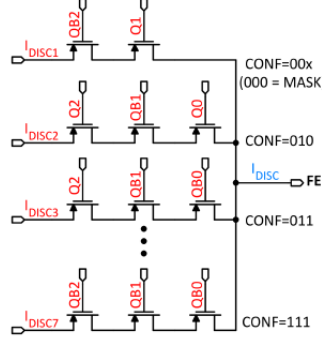


Figure 1.15: Schematic of 3-bit tuning DAC (TDAC)

#### 1.2.2.1 Results from fine tuning

It has been trying to apply the fine tuning method to level out the threshold of some pixels as much as possible.

Results from measurements done later (Ludovico talk TREDI) pre and post

### 1.3 ToT calibration with internal injection

As it has been pointed out in the previous, choosing to use a simple diode instead a PMOS transistor as reset input baseline element, increases the tolerance to TID radiation but at the same time it implicates a non-linear relationship between the injected charge and the ToT. For this reason, one of the target of this analysis consisted to fit the trend (?)  $Q_{inj}$  vs. ToT, in order to obtain the absolute calibration of the whole matrix.

#### 1.3.1 Injection circuit issues

In carrying out the measurements mentioned above, we started to noticed some issues with the injection circuit, which seemed to limit its working range. As a matter of fact the height of the injection pulse is expected to grow linearly increasing the value of charge to be injected. It actually happened up to a value of (about)  $\approx 140$  DAC, but for higher quantities of injected charge, the circuit seemed to increase not only the height of the signal, but also the threshold by a certain amount of  $\Delta V$  (or equivalently of  $\Delta Q$ , related by the conversion factor reported in REFERENCE). Moreover, for injection height grater than 200 DAC, only the threshold grows, without increasing the actual injected charge in any way.

We come to the conclusion that the grows of the threshold was artificial and due to the failure of the injection circuit.[?]

However as we have seen in the previous section (reference), the threshold depends on the settings of the chip registers and it can't be influenced by the injected charge, otherwise the whole response of the chip would be chaotic and it would not be reliable to take precise measurement of the impinging particles.

A method (recipe) has been therefore devised to obtain a reliable values of threshold and ToT up to a value of 170 DAC of effective (actual) charge injected. Moreover the characterization of the function to describe the  $Q_{inj}$  - ToT relationship has allowed also to extrapolated ToT values in the forbidden region of charge by the internal injection circuit issue (above  $\approx 1717 e^-$ ), that usually corresponds to the emission peaks of the radioactive sources available in the laboratory.

### 1.3.2 Time Over Threshold (TOT) curves and fit

The function chosen for this purpose is:

$$y(x) = a \cdot x + b - \frac{c}{x - t} \quad (1.4)$$

with  $a$ ,  $b$ ,  $c$  and  $t$  free parameters and where the  $y$  represents the ToT corresponding to a precise value of collected charge, express by  $x$ .

Actually we know that the ToT distribution starts to grow near the threshold, so a random parameter among them, could be computed in function of the threshold value estimated from the previous measurements, explained (shown, described) in section 1.2.1.

In particular knowing that  $y(x_{th})$  must be equal to 0, that is the ToT at the value of the threshold, it can be imposed:

$$0 = a \cdot x_{th} + b - \frac{c}{x_{th} - t} \Rightarrow c = x_{th}^2 \cdot a + x_{th} \cdot (b - a \cdot t) - t \cdot b \quad (1.5)$$

In this way the number of parameters to fit is reduced.

So the same data collected in the previous measurements of thresholds have been used to fit the ToT curves of all pixels for each frontend, so the registers are set in according to the "GOE" settings (1.1 on page 10 for Normal and Cascode FE and ?? on page ?? for HV's). In table 1.3 are reported the value of the threshold considered for each one of them (so that) to extrapolate the value of the parameter  $c$  and the results of the fit for all parameters. In figure 1.16 on the following page the results obtained for all Normal, Cascode and HVs FE. The parameter  $c$  is chosen only for simplicity of calculation.

	<b>Normal</b>	<b>Cascode</b>	<b>HV Cascode</b>	<b>HV</b>
<i>threshold [DAC unit]</i>	53.62	60.19	35.34	31.70
<i>a</i>				
<i>b</i>				
<i>c</i>				
<i>t</i>				

Table 1.3: Threshold and parameters obtained from the fit of ToT curve for each frontend.

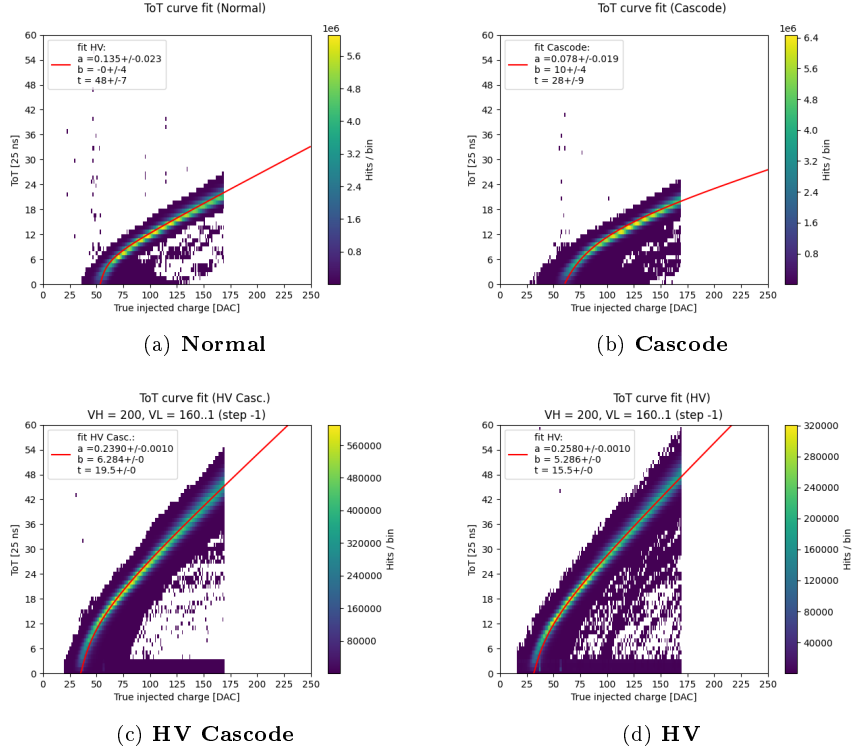


Figure 1.16: ToT curves fit for all frontend.

## 1.4 Response to radioactive source and absolute calibration

The absolute calibration of the matrix consists in characterizing the signal response (conversion gain?) of pixels for each FE. By the means of the  $Q_{inj}$  - ToT fit (section 1.3.2), it is possible to extrapolate (deduce, estimate) the value of the ToT of the signal induced for whatever collected charge. At this point then, three (or four) different X-rays radioactive sources were used to study the signal spectrum and the response time of the matrix, with emission lines from 6 to 60 KeV (1600 to 16000 e-).??? In fact the known energies of the sources emission spectrum (so that the charge released in the matrix from particles emitted in decays) allow to compare the spectra obtained irradiating the chip, with the expected value of their peaks. [Only the events in which all charge inducted is collected in a single pixel are a part of the peaks reconstructed by the chip.] Moreover these radioactive sources allowed to extend the ToT calibration for (at) higher value with respect to the limit imposed by the saturation of the internal injection circuit (section 1.3.1). In table 1.4 on the next page are shown the emission energies of the sources employed, that it was possible to see with the chip under test.

[Considering that the average energy necessary to produce an electron/hole pair in silicon is 3.65 eV, it is possible to convert the peak energies in a mean

value of electrons released by the means of equation on this page. So in the table are reported also the equivalent emission in electrons, which will be useful further.]

$$N_{e^-} = \frac{E [eV]}{3.65 \left[ \frac{eV}{e/h \text{ pair}} \right]} \quad (1.6)$$

Source	Energy $\gamma$ [KeV]	Equivalent charge [ $e^-$ ]
$^{55}\text{Fe}$	5.9	1616
$^{241}\text{Am}$	13.9	3808
$^{241}\text{Am}$	17.7	4849
$^{241}\text{Am}$	20.7	5671
$^{109}\text{Cd}$	22	6027
$^{241}\text{Am}$	26.4	7233
$^{241}\text{Am}$	59.7	16356

Table 1.4: Emission lines of  $^{55}\text{Fe}$ ,  $^{241}\text{Am}$ ,  $^{109}\text{Cd}$  sources visible by the sensor.

### 1.4.1 $^{55}\text{Fe}$

The  $^{55}\text{Fe}$  source decays by **electron capture** to  $^{55}\text{Mn}$ . One of the photons emitted in this transition has an energy of 5.9 KeV ( $K_\alpha$ ) and it produces in turn a photo-electron which deposits a ionization charge of about 1616  $e^-$  in the sensor. All flavors were irradiated with a  $^{55}\text{Fe}$  source available in the laboratory (scrivere caratteristiche). In figure 1.17 on the next page are shown the results obtained. Each peak was fitted by a gaussian function, limited in the region of the peak itself. The hump (shoulder, bump) for smaller ToT is a consequence of charge sharing among pixels.

As it can be seen for the HV's FE a cut has been applied only to make clearly visible the emission line because a lot of noisy pixels caused a sharp peak at 0 ToT. As a matter of fact in this flavors there were several columns of not-functioning pixels. In the box of each plot are also reported the results of the fit that will be crucial in the following.

### 1.4.2 $^{241}\text{Am}$

The  $^{241}\text{Am}$  source has a more complex spectrum (figure 1.18 on the following page) and not all its peaks can be revealed (detected) by the chip (because of the limited range of ToT available, depending on the bit dedicated to it). The spectrum shows other minor peaks besides the usual intense gamma peaks (59.5 and 26.3 keV) and several characteristic L X-rays from  $^{237}\text{Np}$  (20.7, 17.7 and 13.9 keV).

Results are reported in figure 1.19 on page 21. In the case of the first two flavors, it could be possible to fit four peaks of the emission lines. In case of the HV's flavors instead, only three peaks for the HV-Cascode FE and two for the HV.

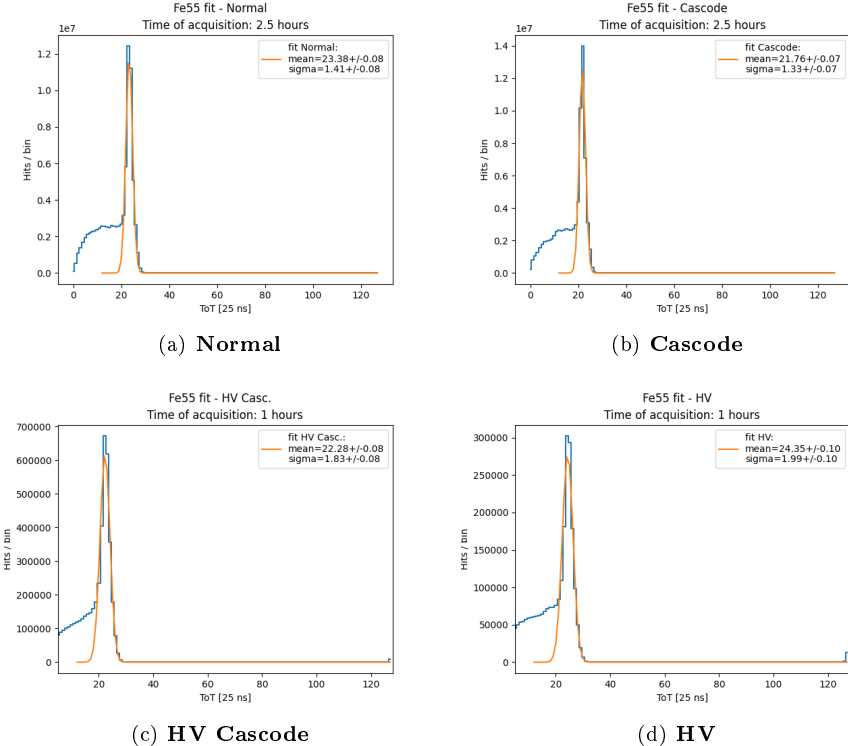


Figure 1.17:  $^{55}\text{Fe}$  peaks for all frontends.

As a matter of fact the AC-coupling causes about 41% of signal loss (reference), so they are much less evident and more difficult to fit as isolated peak.

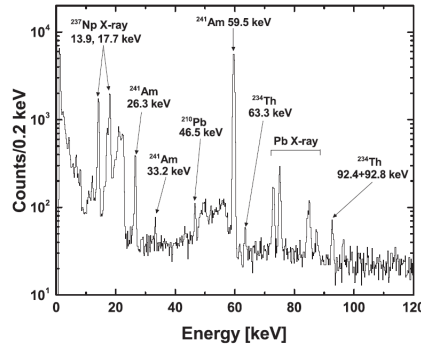


Figure 5. Gamma-ray spectrum of the  $^{241}\text{Am}$  source.

Figure 1.18:  $^{241}\text{Am}$   $\gamma$  emission spectrum.

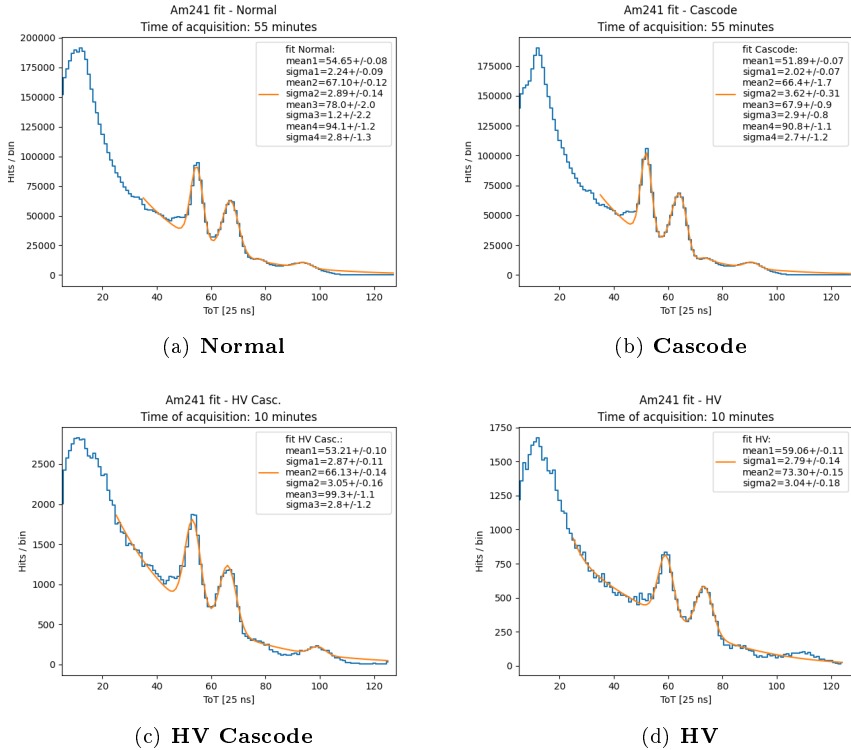


Figure 1.19:  $^{241}\text{Am}$  peaks for all frontends.

### 1.4.3 $^{109}\text{Cd}$

The third source employed was the  $^{109}\text{Cd}$ . This isotope decay in  $^{109}\text{Ag}$  by electronic capture, producing a photon of 22 KeV in the transition. In figure ?? on page ?? the results obtained irradiating all FE.

### 1.4.4 Injection capacitance calibration

Here it's necessary to point out that for iron source more statistics were collected so in this case a complete analysis of each pixel could be done. For the other sources instead, there weren't enough statistics on every pixel so the injection capacitance has been estimate only as a mean value for the whole front-end, just to compare with the results obtained from the iron analysis.

In case of  $^{55}\text{Fe}$  source, we managed to fit the emission peak for each working pixel of the whole matrix. The value of the charge corresponding to the ToT peak of the emission line was extrapolate considering the parameters' values obtained by fitting the  $Q_{inj}$  - ToT relationship (section on page 17).

Specifically the fit function on page 17 was inverted obtaining:

$$x(y) = \left( \frac{t}{2} - \frac{b}{2a} + \frac{y}{2a} \right) \pm \sqrt{\left( \frac{t}{2} + \frac{b}{2a} - \frac{y}{2a} \right)^2 + \frac{c}{a}} \quad (1.7)$$

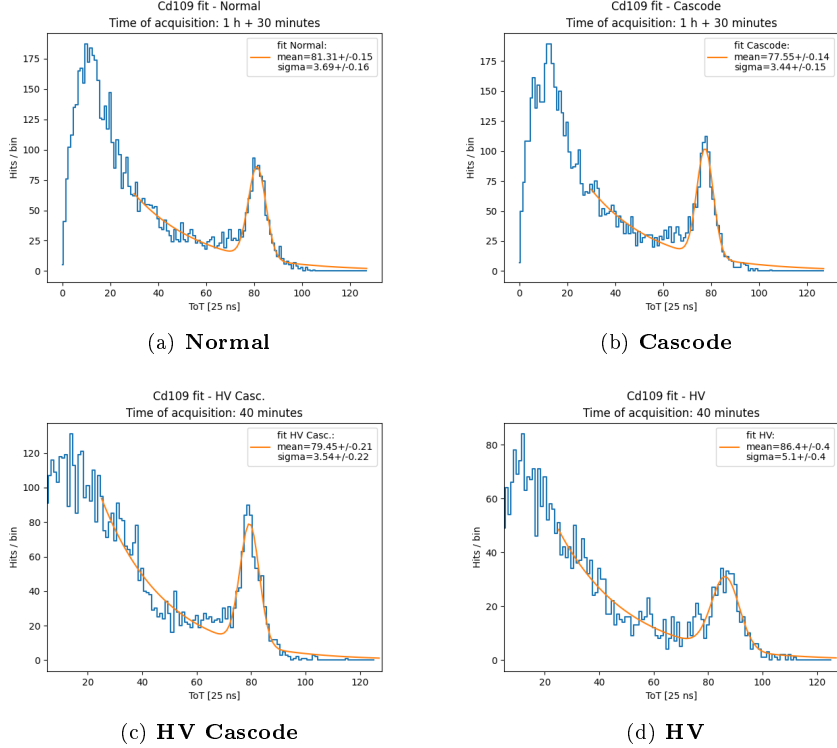


Figure 1.20:  $^{109}\text{Cd}$  pekas for all frontends.

where  $x$  represents the charge corresponding to the ToT labeled by  $y$ .

As shown in table on page 19, the charge released in the sensor (considering that collected from only one pixel) corresponds roughly ( $\approx$ , approximately) to  $1616 e^-$ . Therefore it was possible to calculate (estimate) the conversion factor for each pixel as follows:

$$C_f \left[ \frac{e^-}{DAC} \right] = \frac{1616 e^-}{ToT \frac{DAC}{ToT_{unit}}} \quad (1.8)$$

By these steps, a value of the injection capacitance was estimated for each well-functioning pixel. In figure on the facing page is reported the distributions of the injection capacitance estimated, fitted by a gaussian function.

[As expected the capacitance oh the HV's flavors is much higher than the Normal and Cascode FE? No! It's expected all the same?]

Regarding the other sources, it was impossible to fit the distributions for each pixel due to low statistics. For this reason only a mean value for all flavor could be extrapolate. In table on page 24 the results obtained with the same method used with the iron source, but considering all pixels of each flavor.

Bringing equation on page 8 back to mind, the conversion factors of the flavors are not those expected. In particular for the HV's flavors, this factor is almost the double and it could mean that the injection capacitance is greater than expected. As matter of fact, with respect to Tj-Monopix 1, the prototype

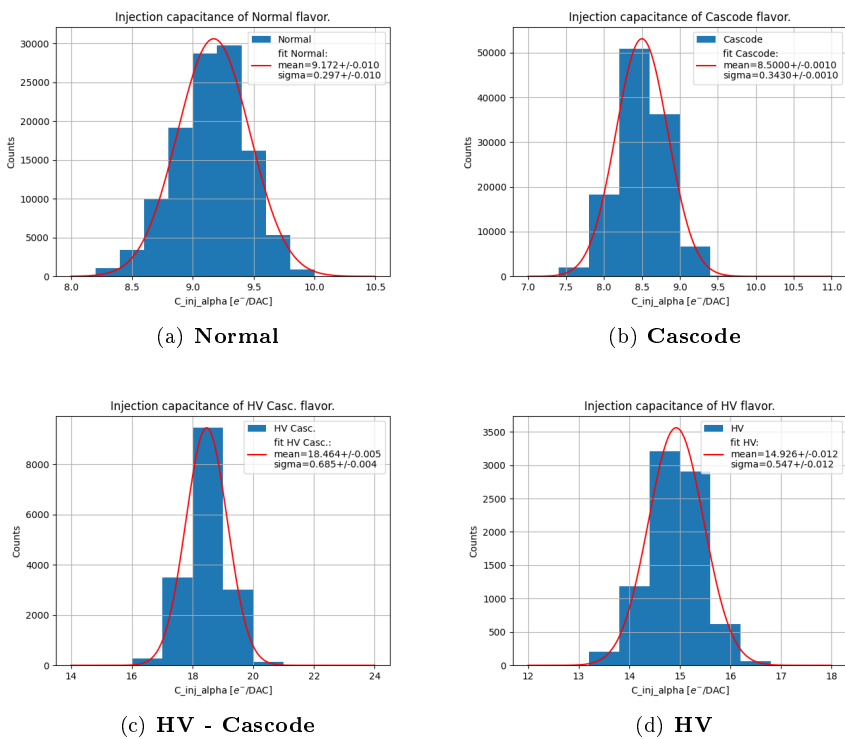


Figure 1.21: Injection capacitance distributions of all FE.

Source peak	$C_{Normal}$	$C_{Cascode}$	$C_{HVCascode}$	$C_{HV}$
$^{55}\text{Fe}$ (5.9 KeV)	9.37	9.00	19.33	18.56
$^{241}\text{Am}$ (13.9 KeV)	8.94	8.91	19.23	18.22
$^{241}\text{Am}$ (17.7 KeV)	9.16	8.84	19.59	18.63
$^{241}\text{Am}$ (20.7 KeV)	9.15	10.11	-	-
$^{109}\text{Cd}$ (22 KeV)	9.32	9.39	20.16	19.6
$^{241}\text{Am}$ (26.4 KeV)	9.60	9.61	19.25	-
Mean value	9.26	9.31	19.51	18.75

Table 1.5: Estimation of injection capacitance of all flavors for different source emission peaks.

under test was design in order to have the same injection capacitance for all flavor, equal to 230 aF.

so? Loss of charge?

It's necessary to consider that maybe some measurments were done in different conditions of pressure and temperature?

#### 1.4.5 Check on linearity of tot fit

In the end all emission peaks from the several sources have been plotted for each frontend in order to verify the agreement between their trend and the ToT-Q relationship studied by the internal injection.

At first the charge corresponding to the electrons expected to be released for each peaks, has been calculated with the nominal conversion factor equal to  $10.1 \frac{e^-}{DAC}$ . As it could be seen from results in figure on the next page there isn't good agreement between data and ToT relationship obtained(learnt) in section on page 17.

After the calibration instead, assuming the average value of injection capacitance calculated in table on page ??, the charge corresponding to the emission peaks have been recalculated and results are shown in figure on page 26.

After(through) the calibration a better agreement is therefore obtained.

### 1.5 Operation with low threshold

One of the most important target of the chip design is to keep high efficiency even after irradiation damage. All experimental environments in fact(indeed) are exposed to high doses of radiations, so it's crucial to make sure the functionality of the irradiated detectors.

For this reason, many tests were done in order to understand the chip behaviour at lower threshold that allowed to keep(maintain) good value of efficiency. Moreover working at low threshold allowed to detect low charge events due to charge sharing or charge trapping (effect which increased after irradiation), especially in case of thin epitaxial material.

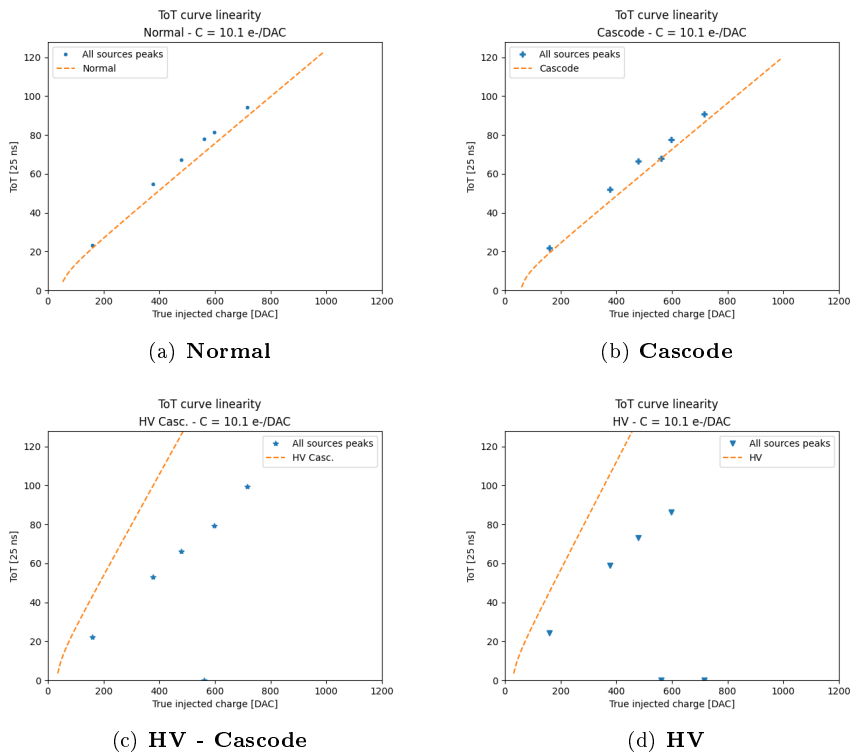


Figure 1.22: ToT linearity of all flavors assuming the nominal(expected) conversion factor equal to  $10.1 \frac{e^-}{DAC}$ .

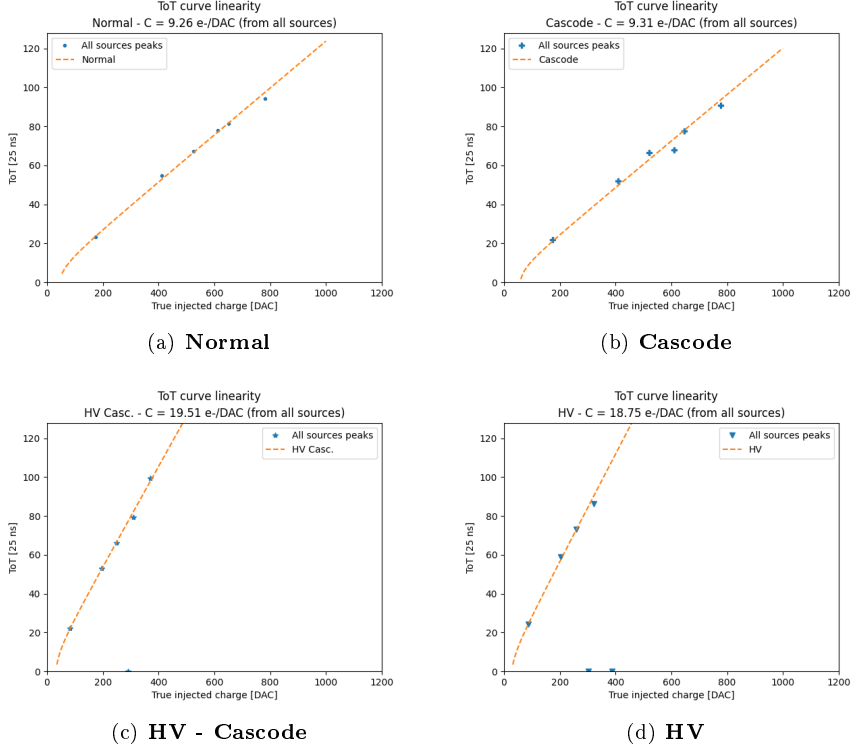


Figure 1.23: ToT linearity of all flavors assuming the conversion factor obtained from calibration for each FE.

### 1.5.1 Register optimization

As we have seen in section (REFERENCE), there are a lot of registers which control the discriminator threshold and also the readout sequence. So preliminary it was necessary to run some tests exploring their settings in order to operate the chip at(or with) lower thresholds.

Now we will go through the main registers used for this purpose, in order to explain their functionality. There are several dozens of registers but we focused on some of the most important and crucial to set the threshold:

- $I_{CASN}$  : this current is responsible of the output baseline signal[set the baseline of the FE output and change the thr] that goes to the input discriminator. In a few words, higher this value, higher the baseline, lower the threshold and also a little bit the gain. [Vice versa, decreasing this register's value.]
- $I_{THR}$ : it controls the pre-amplifier feedback strength and speed, so it's responsible for the output reset rate. Increasing  $I_{THR}$  results to lower gain and faster return to baseline, so higher threshold. (This value is preferably set to 8nA in order to avoid high ToT slope).
- $I_{DB}$ :

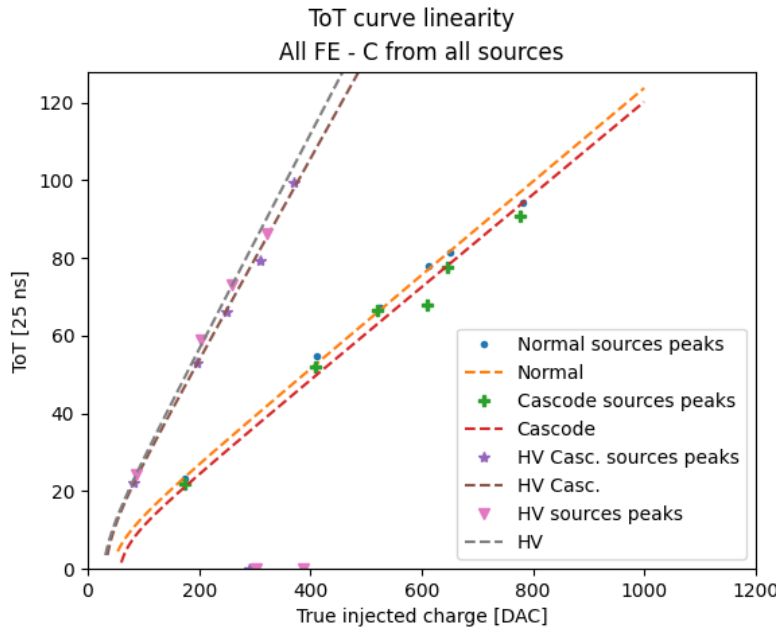


Figure 1.24: Summary of trends.

- $I_{TUNE}$ :
- $I_{BIAS}$ :
- $V_{RESET}$ :

### 1.5.2 Comparison between data and simulation

In the interest of understanding how the settings of the chip influence the threshold's value, several measurements have been taken varying the values of the main registers which are responsible for it. The results are compared with simulations done by Hung Pham (...). [??]

#### 1.5.2.1 $I_{CASN}$

This current is responsible of the output baseline. In a few words, higher this value, higher the baseline, lower the threshold and also a little bit the gain.

In figure 1.25 on the next page, we can see the simulated behaviour of the threshold and the gain, increasing the value of  $I_{CASN}$ .

To verify the trend of threshold in particular, three different acquisition have been taken by fixing  $I_{THR} = 20, 40, 64$  and increasing  $I_{CASN}$  from 0 to 30 DAC, with a step of 5 DAC. We have done this enabling 200 pixels in the Cascode FE (rows: 472 - 512, cols: 225 - 230).[??]

The threshold distributions have been fitted with a gaussian function for each measurement, in order to obtain the average values and their dispersion.

In figure 1.26 all trends obtained from these data are reported.

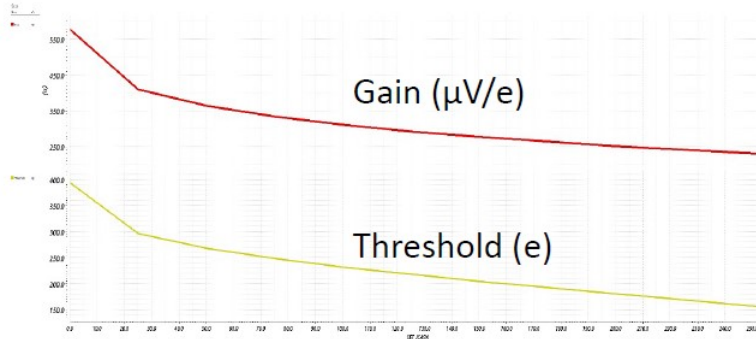


Figure 1.25: Trends of Gain and Threshold increasing  $I_{CASN}$ .

[TREND OF DISPERSION?]

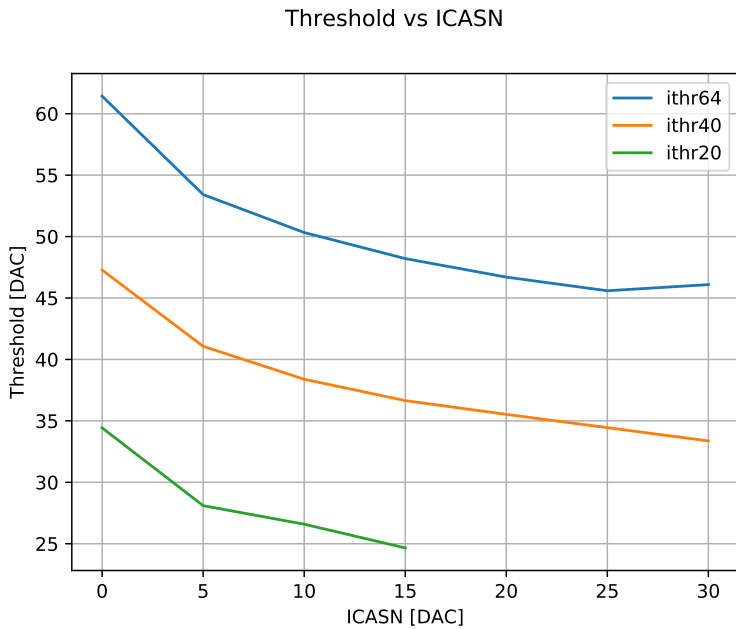


Figure 1.26: Threshold vs.  $I_{CASN}$  for  $I_{THR}= 20, 40, 64$ .

### 1.5.2.2 $I_{THR}$

Reusing the same data of the previous measurements, the trend of the threshold have been studied, changing the value of  $I_{THR}$  and fixing that of  $I_{CASN}$ . In this case only  $I_{CASN}$  from 0 to 15 DAC is considered, because for higher values we don't have enough measures of the threshold (specifically only two for  $I_{THR}=40, 64$ ). The results are shown in figure 1.27 on the next page.

We can compare them with the simulation done by Hung Pham in figure 1.28.

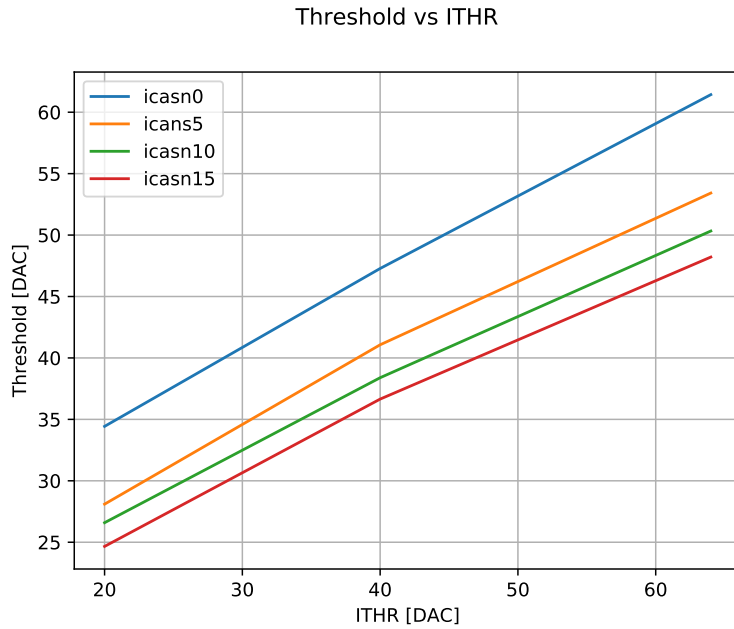


Figure 1.27: Threshold vs.  $I_{THR}$  for  $I_{CASN} = 0, 5, 10, 15$ .

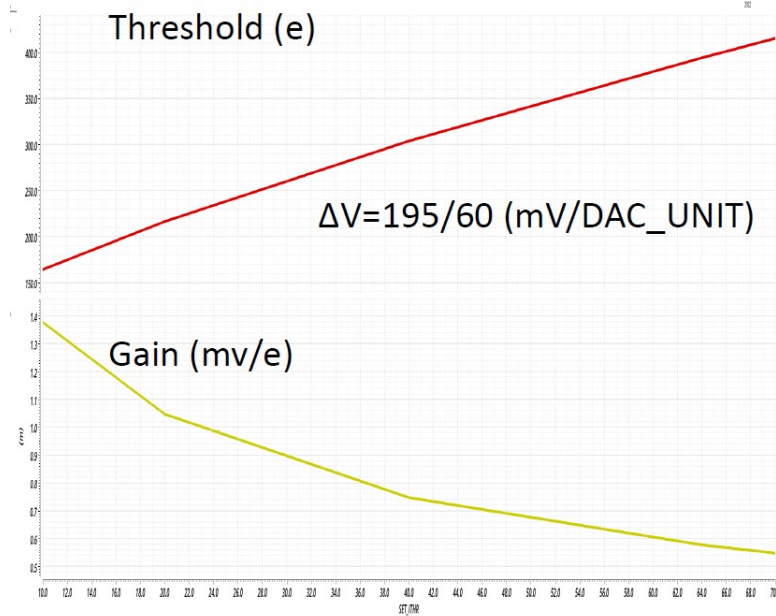
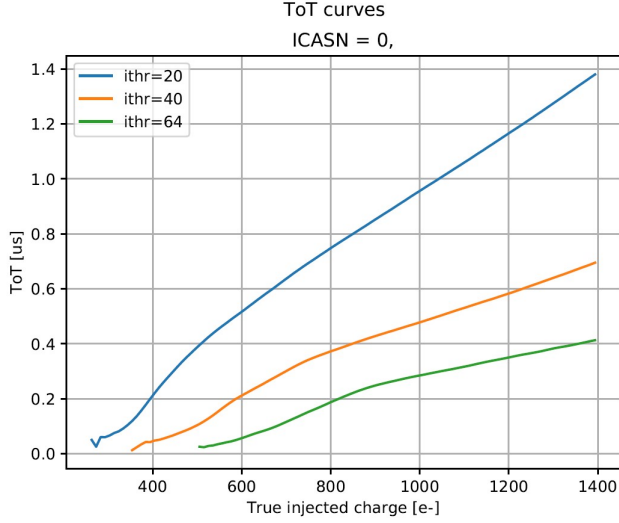


Figure 1.28: Trends of Gain and Threshold increasing  $I_{CASN}$ .

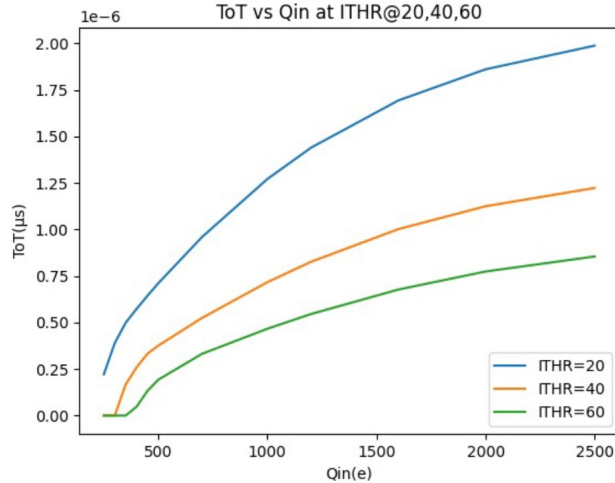
### 1.5.2.3 Time over Threshold (ToT)

The last analysis done in order to make a comparison with the simulations, is about the trend of the ToT changing the value of  $I_{CASN}$  for a fixed value of

$I_{THR}$  and vice versa. In particular we consider the data obtained with  $I_{CASN}$  fixed to 0 DAC and  $I_{THR}$  to 64 DAC, which are the values studied and used for this registers during the Test Beam in Desy.



(a) ToT vs  $I_{THR}$  ( $I_{CASN}=0$  DAC) - Data (Cascode)

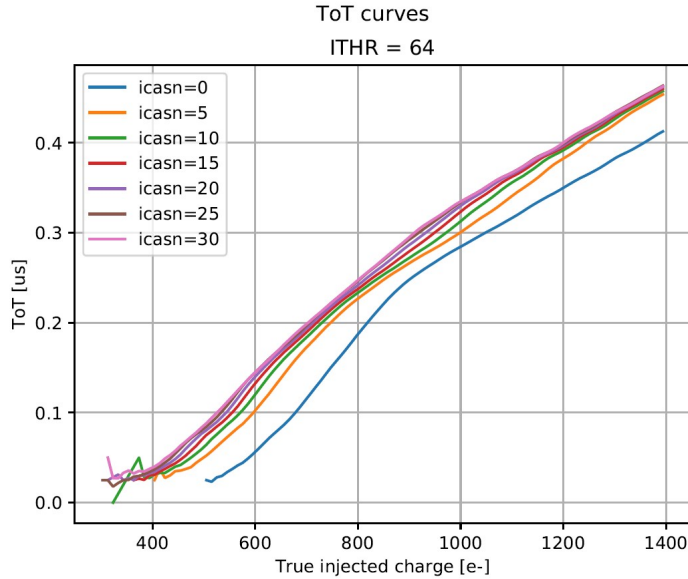


(b) ToT vs  $I_{THR}$  ( $I_{CASN}=0$  DAC) - Simulation

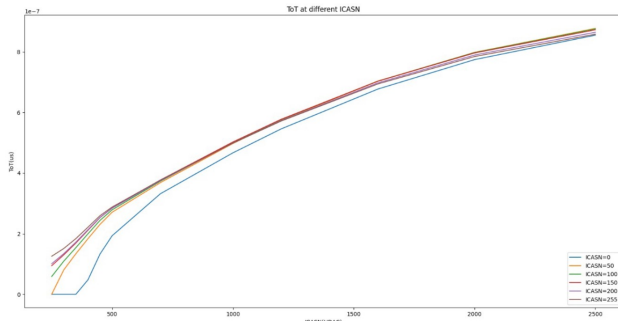
Figure 1.29: ToT vs  $I_{THR}$

#### 1.5.2.4 some nice picture of the optimized thr and tuning

!!!!!!



(a) ToT vs  $I_{CASN}$  ( $I_{THR}=64$  DAC) - Data (**Cascode**)



(b) ToT vs  $I_{CASN}$  ( $I_{THR}=64$  DAC) - Simulation

Figure 1.30: ToT vs  $I_{CASN}$

## 1.6 Cross talk issue and mitigation

### 1.6.1 Hot pixel issue and strategy?

### 1.6.2 Readout sequence

### 1.6.3 Hot pixel strategy (study)

### 1.6.4 Cross-talk

### 1.6.5 Mitigation

## 1.7 Test Beam results

## 2. Conclusions

# List of Figures

1.1	The W14R12 chip tested during the Test Beam in Desy . . . . .	5
1.2	Detection efficiency map of a TJ-Monopix1 chip with 25 $\mu\text{m}$ p-epitaxial layer that has been irradiated to $10^{15} n_{eq}/cm^2$ NIEL.	5
1.3	The layout of the TJ-Monopix2 prototype divided in four different flavors: <b>Normal</b> , <b>Cascode</b> , <b>HV-Cascode</b> and <b>HV FE</b> . . . . .	6
1.4	Layout of a TJ-Monopix 2 2x2 pixel core. In blue the analog area and in yellow the digital one. . . . .	7
1.5	An example of the S-Curve fitted by the CDF to evaluate threshold and noise. . . . .	9
1.6	S-curves of all pixels of the Normal FE with an injection pulse of 140 DAC. . . . .	10
1.7	Normal FE. . . . .	11
1.8	S-curves of all pixels in the <b>Cascode</b> flavor with an injection pulse of 140 DAC. . . . .	11
1.9	Cascode FE. . . . .	12
1.10	S-curves of all pixels in <b>HV Cascode</b> flavor with an injection pulse of 140 DAC. . . . .	13
1.11	HV Cascode FE. . . . .	13
1.12	S-curves of all pixels in <b>HV Cascode FE</b> with an injection pulse of 140 DAC. . . . .	14
1.13	HV Normal FE. . . . .	14
1.14	HV's FE. . . . .	14
1.15	Schematic of 3-bit tuning DAC (TDAC) . . . . .	16
1.16	ToT curves fit for all frontend. . . . .	18
1.17	$^{55}\text{Fe}$ peaks for all frontends. . . . .	20
1.18	$^{241}\text{Am}$ $\gamma$ emission spectrum. . . . .	20
1.19	$^{241}\text{Am}$ peaks for all frontends. . . . .	21
1.20	$^{109}\text{Cd}$ pekas for all frontends. . . . .	22
1.21	Injection capacitance distributions of all FE. . . . .	23
1.22	ToT linearity of all flavors assuming the nominal(expected) conversion factor equal to $10.1 \frac{e^-}{DAC}$ . . . . .	25
1.23	ToT linearity of all flavors assuming the conversion factor obtained from calibration for each FE. . . . .	26
1.24	Summary of trends. . . . .	27
1.25	Trends of Gain and Threshold increasing $I_{CASN}$ . . . . .	28
1.26	Threshold vs. $I_{CASN}$ for $I_{THR}= 20, 40, 64$ . . . . .	28
1.27	Threshold vs. $I_{THR}$ for $I_{CASN}= 0, 5, 10, 15$ . . . . .	29
1.28	Trends of Gain and Threshold increasing $I_{CASN}$ . . . . .	29

1.29	ToT vs $I_{THR}$	30
1.30	ToT vs $I_{CASN}$	31

## List of Tables

1.1	Settings of the main registers used for all flavors (W14R12 chip) during the Test Beam in Desy. . . . .	10
1.2	Summary table of threshold and noise values for all flavors of the W14R12 chip. . . . .	15
1.3	Threshold and parameters obtained from the fit of ToT curve for each frontend. . . . .	17
1.4	Emission lines of $^{55}\text{Fe}$ , $^{241}\text{Am}$ , $^{109}\text{Cd}$ sources visible by the sensor. . . . .	19
1.5	Estimation of injection capacitance of all flavors for different source emission peaks. . . . .	24